Low Temperature Aqueous Synthesis of Size-Controlled Nanocrystals Through Size Focusing: A Quantum Dot Biomineralization Case Study

Journal:	*Nanoscale*
Manuscript ID	NR-ART-07-2018-006166.R1
Article Type:	Paper
Date Submitted by the Author:	08-Oct-2018
Complete List of Authors:	Spangler, Leah; Lehigh University, Chemical and Biomolecular Engineering Cline, Joseph; Lehigh University, Materials Science and Engineering Kiely, Christopher; Lehigh University, Materials Science and Engineering McIntosh, Steven; Lehigh University, Chemical and Biomolecular Engineering

Low Temperature Aqueous Synthesis of Size-Controlled Nanocrystals Through Size Focusing: A Quantum Dot Biomineralization Case Study

Leah C. Spangler[1], Joseph Cline[2], Christopher J. Kiely[1,2], Steven McIntosh*[1]

[1] Department of Chemical and Biomolecular Engineering, Lehigh University, Bethlehem, PA 18015, USA.

[2] Department of Materials Science and Engineering, Lehigh University, Bethlehem, PA 18015, USA.

*mcintosh@lehigh.edu

Abstract

Traditional quantum dot synthesis techniques rely on the separation of nucleation and growth to control nanocrystal size. However, the same goal can be achieved through slow and continuous introduction of reactive precursors to keep the growth mechanism in the size focusing regime throughout synthesis. In this work, we demonstrate the efficacy of this approach within the framework of functional material biomineralization where, despite simultaneous nucleation and growth of particles, this growth mechanism enables size-controlled nanocrystal synthesis. Herein, the single enzyme cystathionine γ-lyase (CSE) is utilized to biomineralize CdS nanocrystals via the slow, but continuous turnover of the amino acid L-cysteine to produce H_2S. Nanocrystal nucleation and growth theories confirm that consistent addition of monomers will result in a high supersaturation term, driving the nanocrystal growth mechanism into the size focusing regime. We further confirm this theory by mimicking biomineralization via chemical routes and demonstrate the influence of varying supersaturation, to further control the average nanocrystal size. Finally, altering the chelation strength of the capping agent L-cysteine is found to play a key role in balancing nanocrystal growth in solution and long-term stability.

Introduction

Quantum confined semiconductor nanocrystals, or quantum dots, are critical materials for energy, catalyst, display, and biomedical applications due to their size controllable optoelectronic properties. Monodisperse colloidal nanocrystal populations are typically obtained using the “hot-injection” organometallic synthesis route, which separates nucleation and growth processes; a rapid

introduction of chemical precursors causes an instantaneous nucleation of uniformly sized particles, followed by subsequent growth of the nanocrystals without the addition of supplementary monomers.[1-3] We have recently developed a single enzyme, aqueous phase, room temperature, biomineralization approach to produce application quality quantum dots through a more environmentally benign and lower cost synthesis. Intriguingly, this approach leads to size-controllable, uniform populations of nanocrystals despite the stark deviation from typical synthesis methods.[4] The biomineralization approach leads to concurrent nucleation and growth due to the continuous generation of reactive precursors throughout the growth process. At first consideration, this would be expected to lead to polydispersity in the size distributions due to secondary nucleation of nanocrystals. In this work, we explain this surprising result by applying established nanocrystal nucleation and growth theory to the case of controlled, slow and continual introduction of the reactive precursor, utilizing CdS quantum dot biomineralization as a case study.

A complete theory for colloidal nanocrystal growth, developed by Peng et al., can be used to model the effect of experimental synthesis parameters on the evolution of particle size distributions.[5] This model demonstrates that nanocrystal growth under diffusion controlled conditions will occur in two regimes depending on the availability of monomers in solution, and can be evaluated by analyzing the peak widths of the absorbance and photoluminescence spectra for a population of nanocrystals. The first growth regime, size focusing, occurs when monomers are still available in solution and particle growth can occur by monomer addition. The second regime, size broadening, occurs when all the monomers are consumed, and large particles grow at the expense of dissolving smaller crystals, also known as Ostwald ripening.[6, 7] In relation to the nanocrystal optical properties, this results in narrowing or broadening of the absorbance and fluorescence peak widths, respectively.[5, 8] Because of the rapid consumption of monomers in the “hot-injection” technique, size broadening is frequently observed during subsequent nanocrystal growth.[9] If the monomers concentration is maintained, size narrowing behavior would be expected if the nucleation of new particles is suppressed.[10]

Although organometallic synthesis methods produce high quality nanocrystals, they present barriers to manufacturing quantum dots at the extremely large scale required to impact, for example, global energy demand. These techniques require elevated temperatures, utilize solvent-based processing with often toxic or pyrophoric precursors, and are usually conducted under inert atmosphere in batch mode.[11] Biomineralization, the process by which organisms generate minerals, has recently been applied as a low cost, environmentally benign method for the aqueous phase, ambient temperature, and often aerobic, synthesis of metal chalcogenide semiconductor nanocrystals.[12] The

process utilizes enzymatic pathways present organisms such as yeasts or bacteria to produce reactive chemical species from inert biological precursors.[13-16] Biomineralization of semiconductor nanocrystals can also be achieved by utilizing engineered proteins to template mineralization from a chemical reaction.[17, 18] However, in order to create functionally useful quantum confined nanocrystals, the process must not only produce particles with the correct crystal phase and composition, but also with a reasonably narrow size distribution in the quantum confined range.

We have recently demonstrated perhaps the conceptually simplest feasible biomineralization process for size-controlled metal chalcogenide quantum dots using a single engineered enzyme in the presence of the precursor metal salts and chalcogenide containing amino-acids.[4, 19] Most commonly, we have utilized a Cystathionine γ-lyase (CSE) to generate reactive sulfur species from L-cysteine in the presence of metal acetate in the aqueous phase under aerobic conditions at 37 °C. The enzyme was initially derived from an engineered form of *Stenotrophomonas maltophilia* but more recently is produced in a commercially viable route through expression in *E. coli*. This approach has been applied to the size-controlled formation of a range of single metal sulfides, alloys, and core-shell heterostructures with the materials demonstrated in applications from quantum dot sensitized solar cells to bioimaging.[20-22]

This single enzyme approach stands in contrast to previous biomineralization methods in several ways; the time for quantum dot synthesis is reduced to 1-5 hours as opposed to 24-72 hours typically required by bacteria or yeast, and the use of a single enzyme as opposed to an entire organism allows for a simpler and cleaner synthesis approach with little or no post-purification required. Most importantly, however, is the ability of CSE to synthesize size controllable quantum dots with relatively uniform populations. This differs from the wide size distribution typically achieved by biomineralization through single protein templating and is surprising given the mechanism for nanocrystal synthesis; CSE slowly converts the amino acid L-cysteine to H_2S, which should result in the continuous nucleation of new nanocrystals throughout the growth period.

There have been a few similar reports of aqueous CdS synthesis that utilize slow sulfur introduction by decomposing sulfur precursors such as thiourea or MPA at high temperatures (100-200 °C) and pressures.[9, 23] While the slow introduction of sulfur is similar to our synthesis method, the elevated temperature alters the growth kinetics of the nanocrystals when compared to our room temperature synthesis and size broadening is frequently observed. Several groups have demonstrated the mineralization of CdS nanocrystals at room temperature through the addition of cadmium and a reactive sulfur source, such as Na_2S in the presence of capping agents such as TGA, MPA, or short chain

peptides.[9, 17, 18] However, size control is only obtainable by altering the capping agent; otherwise, a broad size distribution is obtained, resulting in a reduction quantum dot quality unless post-processing steps, such as size exclusion chromatography, are used.

While we have previously pointed to a role of the enzyme in controlling the synthesis[4], and discussed the influence of growth conditions on the growth process[24], herein we explore the fundamental difference between the high temperature rapid growth achieved by hot-injection techniques and the low and slow approach characteristic of biomineralization. We believe these insights will have important implications for the future development of scalable biomineralization of nanomaterials.

Experimental Methods

Expression and Purification of Recombinant CSE

The identification and engineering of the CSE enzyme for simplified expression in E. coli has been presented previously.[4] Briefly, a putative form of the *S. maltophilia* CSE identified from the mass spectrometry results was optimized with E. coli codons (Smal_0489 Genscript), subcloned into pET28a (+), and transformed into BL21. The enzyme was then produced using typical expression protocols. In summary, the transformed BL21 cells were sub-cultured into 200 mL of lysogeny broth with 50 μg/mL Kanamycin antibiotic and grown at 37 °C for 12-24 hours. The BL21 cells were then re-suspended in fresh lysogeny broth with 50 μg/mL Kanamycin and 1 mM IPTG to induce expression. The expression was performed at 20 °C for 10 hours. Following expression, the BL21 cells were harvested using centrifugation at 3000 x g, resuspended in lysis buffer (10 mM imidazole, 100 mM HEPES, 500 mM NaCl, 10% glycerol), and sonicated on ice at 12 W for 10 seconds on/10 seconds off. The enzyme containing supernatant was separated from cell debris using centrifugation and then purified using immobilized metal affinity chromatography (IMAC). The IMAC column contained Ni-NTA chelating sepharose (GE Healthcare) and the cell lysate was eluted using increasing concentrations of imidazole buffer (20 mM HEPES, 500 mM NaCl, 10% glycerol, and 10-500 mM imidazole). CSE was stored in imidazole buffer until use.

Single Enzyme Biomineralization of CdS Quantum Dots using CSE

CdS quantum dots were synthesized by the single enzyme cystathione γ-lyase (CSE) as previously reported. [4] Quantum dot synthesis was initiated by combining 1 mM Cd acetate (Alfa Aesar, 99.999%

Puratronic), 8 mM L-cysteine (8 mM, Spectrum Chemicals), and 0.05 mg/mL CSE in 0.1 M Tris-HCl (pH 7.5 or 9, VWR). The solutions were incubated at 37 °C for various times between 1-5 hours.

Chemical synthesis of CdS

A solution of cadmium acetate and L-cysteine in Tris buffer (pH 7.5) was placed into a 4 mL cuvette with a stir bar. Sodium hydrosulfide (NaHS, Sigma-Aldrich) was then quickly pipetted into the cuvette while stirring and allowed to react for 1 minute before removing from the stir plate for measurement. Incubation of the solution was performed in an incubator at 37 °C with shaking to ensure even mixing. The titration experiments were performed as above with a few minor changes: the NaHS was added in 2 μM increments with 1 minute of stirring between each addition. The solutions were kept at room temperature throughout the experiment. UV-vis measurements were recorded after the addition of every 10 μM NaHS.

Quantification of H_2S using the AzMC Assay

The procedure for detecting H_2S using 7-azido-4-methylcoumarin (AzMC) was followed as reported by Thorson et al.[25] In summary, AzMC (Sigma-Aldrich, 97%) was dissolved in DMSO (Fisher) and diluted to a final concentration of 10 μM in activity buffer (200 mM Tris HCl pH 8, 5 μM pyridoxal 5'-phosphate (PLP), 10 mM glutathione, and 0.5 mg/mL BSA). Fluorescence measurements were recorded using a Tecan Infinite M200 plate reader with an excitation wavelength of 365 nm and an emission wavelength of 450 nm. A standard curve was produced by adding known concentrations of NaHS to the assay solution and measuring the corresponding fluorescence. The assay was performed with 2.5 mM L-cysteine and 0.015 mg/mL CSE and measured every 8 minutes over 90 minutes. Each sample was replicated in triplicate.

Characterization

Absorbance measurements were collected using a UV-Vis 2600 spectrophotometer equipped with an ISR-2600-Plus integrating sphere attachment (Shimadzu). Photoluminescence experiments were performed using a QuantaMaster™ 400 (Photon Technology International). TEM samples were examined using an aberration corrected JEOL ARM 200CF analytical electron microscope operating at 200 kV equipped with a JEOL Centurio X-ray energy dispersive spectroscopy (XEDS) system.

Results

The enzyme induced biomineralization process utilizes the enzymatic turnover of L-cysteine to form H_2S by the CSE enzyme, a known function of this class of enzymes.[26] In water at a pH ≥ 7.5, thermodynamic stability constants dictate that the H_2S will dissociate to form HS^- and H^+.[27] This active HS^- can then subsequently react with the metal precursor in solution, in this case cadmium, to form the metal sulfide. Thus, the likely primary function of CSE is to generate a reactive sulfur source during synthesis. Note that L-cysteine must be present in excess as it also acts as a capping agent to aid in controlling the growth and stabilizing the nanocrystals in solution.[4, 28]

The rate of H_2S production by CSE quantified in the absence of cadmium using an AzMC assay is presented in Figure 1 a). Even after 90 minutes, the cumulative concentration of H_2S generated, 25.3 μM, is substantially lower than the total amount of cadmium precursor typically used for synthesis, 1 mM. Thus, H_2S will be the limiting mineralization reactant and during the entire synthesis process.

Incubation of cadmium acetate, L-cysteine, and CSE in Tris buffer at pH 7.5 produces solutions with absorbance and photoluminescence spectra consistent with the formation of CdS quantum dots with sizes between 1-3 nm, Figure 1 b) and c). The expected particle sizes of the CdS nanocrystals can be estimated based on the method of Yu *et al* using the absorbance spectra for each population of particles.[30] The calculated particle size for each spectrum are shown in the inset of Figure 1 b). The spectroscopic data was also used to estimate size distributions for the nanocrystal populations by analyzing the HWHM of the absorbance peaks, Table S1, and FWHM of the photoluminescence peaks, inset of Figure 1 c). The HWHM and FWHM values remain mostly constant over the growth time, demonstrating that the size distribution remains consistently narrow throughout growth.

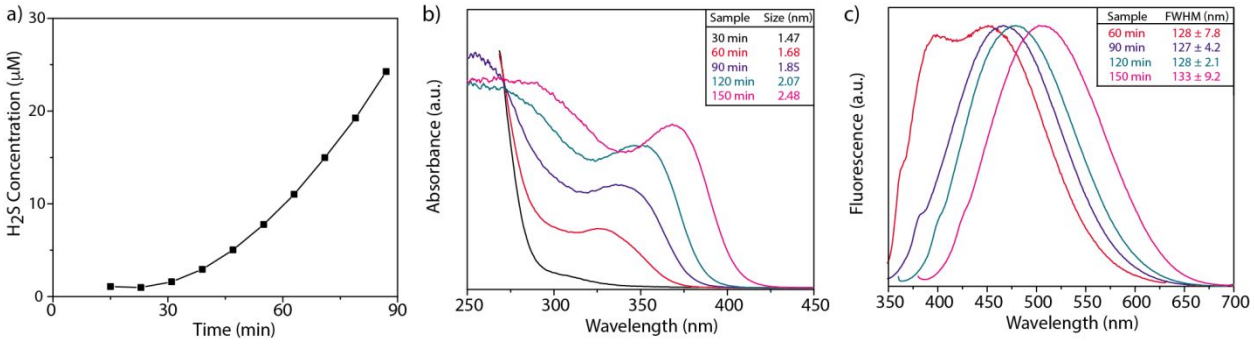

Figure 1. a) Total concentration of H_2S produced by CSE over time, measured using an AzMC assay. b) Typical absorbance and c) photoluminescence spectra for CdS quantum dots synthesized using 0.05 mg/mL CSE. An overlap with fluorescence from CSE (~390 nm) slightly obscures the peak at 60 minutes.

We have previously clearly demonstrated the formation of these quantum dots and their relatively narrow size distributions; for example, average particle diameter and size distributions were calculated from TEM images for CdS populations with absorbance peaks at 320 nm, 350 nm, and 370 nm, and found to be 2.75 $\pm$ 0.68 nm, 3.04 $\pm$ 0.75 nm, and 3.36 $\pm$ 0.95 nm, respectively.[4, 29] HAADF-STEM analysis was performed to examine the average particle sizes and size distributions for the biomineralized CdS nanocrystals shown in Figure 1. The average sizes were calculated to be 2.06 $\pm$ 0.52 nm and 2.40 $\pm$ 0.51 nm for the particles grown for 60 and 120 minutes, respectively. The histograms of the calculated particle sizes are shown in Figure 2. The increase in average particle size at longer growth times correlates with the absorbance peak shift from 330 nm to 350 nm shown in Figure 1 b). The average nanocrystal diameters are slightly larger than the calculated values from the relation of Yu *et al*. This is likely a result of the slightly irregular shape of our as synthesized nanocrystals, previously observed in our enzymatic synthesis. [4, 9] The crystallinity of the CdS nanocrystals was further confirmed using higher resolution HAADF-STEM imaging; representative images are shown in Figure S1. We have previously utilized these such images to fit the lattice spacing and angles to the expected crystal phases of CdS.[4,29]

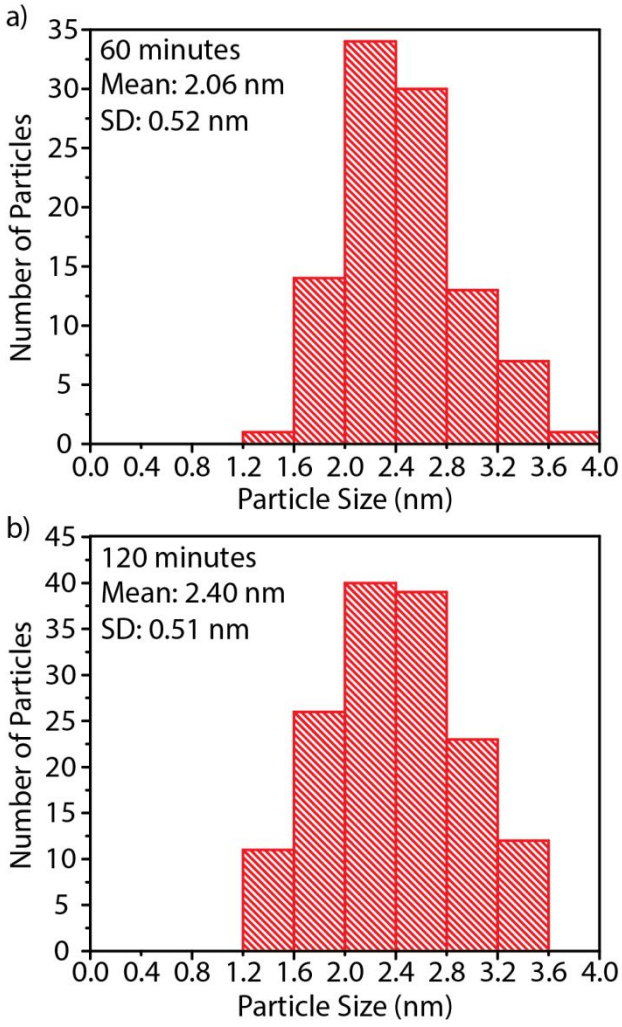

Figure 2. Particle size distributions for biomineralized CdS QDs corresponding to UV-vis absorbance peaks at 330 nm and 350 nm, representative of the populations grown for 60 and 120 minutes in Figure 1 b).

The preservation of a relatively narrow size distribution during the biomineralization process is perhaps surprising given the synthesis conditions. The slow growth by biomineralization occurs at low temperature with continual generation of the reactant, in stark contrast to the typical high temperature hot-injection route, where rapid initial consumption of the limiting reactant is key. From this, one may consider that biomineralization would lead to poor size control, and large size distributions, due to the continuous nucleation of particles induced by the slow and continual generation of the limiting reactant.

To further study the nucleation and growth mechanism without the potential kinetic complications of the enzymatic precursor generation, we employed sodium hydrosulfide, NaHS, so as to accurately control the concentration of HS^- in solution relative to cadmium acetate and L-cysteine. This also enables accurate control over the timing of NaHS addition; *i.e.* added at one time (single-step addition) or introduced slowly over time during synthesis to more closely mimic the biomineralization conditions (titrated addition). The precursor NaHS was chosen because it is a safer alternative to H_2S, and will form H_2S once in contact with water.[31, 32] The temperature was kept at room temperature or 37 °C depending on the experimental set-up, and the other precursor concentrations and buffers were the same as used for enzymatic synthesis.

Instantaneous, single step addition of NaHS leads to significant difference in nanocrystal optical properties when compared with the biomineralization approach. The added NaHS concentrations were scaled up from the H_2S production rate observed in Figure 1 a) to account for the typically higher enzyme concentrations used during synthesis, which is approximately three times the concentration used for the assay. Figure 3 shows the absorbance spectra of the CdS quantum dots formed in solution as a function of initial NaHS concentration immediately following NaHS addition, Figure 3 a), and after a 2 hour dwell at 37 °C, Figure 3 b). The results in Figure 3 show an increase in average particle size for solutions with a higher starting concentration of NaHS. Additionally, the growth behavior following this instantaneous addition is influenced by the initial concentration of NaHS precursor. Nanocrystals synthesized with NaHS concentrations greater than or equal to 300 μM have a starting absorbance peak of 330-340 nm, corresponding to an expected diameter of 1.69-1.75 nm[30], and show continuous peak shifting at other time points measured during growth. These particles also show size focusing behavior during growth, demonstrated by a narrowed absorbance peak width after 2 hours of growth at 37 °C relative to the initial peak; for example, the absorbance peak corresponding to 400 μM NaHS has an initial HWHM of approximately 31 ± 1.1 nm, which is reduced to 23 ± 0.8 nm after 2 hours ripening. This suggests that the concentration of precursors in solution, namely HS^-, is high enough to sustain growth by monomer addition, as opposed to the dissolution of smaller particles to feed the larger particles. The expected particle sizes for all the absorbance spectra are shown in the inset tables of Figure 3. A complete list of calculated HWHM values are presented in Table S2.

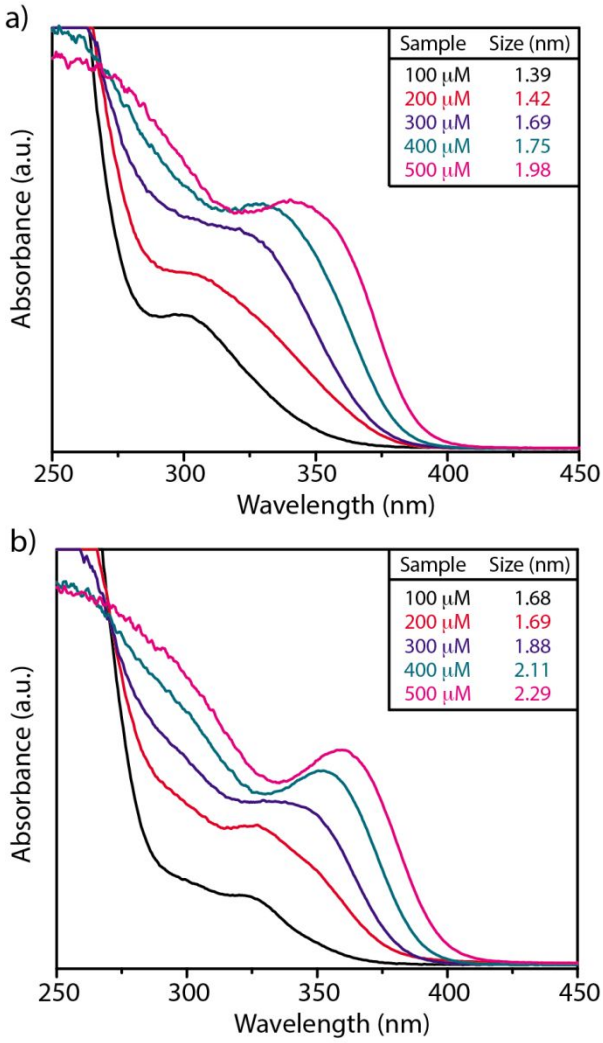

Figure 3. The absorbance spectra for solutions of CdS clusters formed in an aqueous solution of 1 mM Cd acetate, 8 mM L-cysteine, by instantaneous addition of NaHS a) immediately after mixing and b) after 2 hours at 37 °C. Inset tables give estimated CdS nanocrystal diameter and calculated HWHM values for each absorbance peak.

Particle growth for nanocrystals with a starting NaHS concentration 200 μM or less demonstrate discrete peak shifts from ~300 to ~330 nm, as opposed to the continuous peak shift observed at higher starting concentrations of NaHS. Vossmeyer *et al.* also observed discontinuous growth to the same absorbance peaks at 300 and 330 nm for CdS nanocrystals synthesized at low precursor concentrations under analogous synthesis conditions. They proposed that these peaks corresponded to small thermodynamically favored CdS clusters with approximate radii of 0.7 nm and 0.9 nm respectively.[33] In our synthesis, the lowest concentrations of NaHS (100 and 200 μM) have initial absorbance peaks at

approximately 300 and 310 nm, respectively, with a relatively sharp shoulder for the lower concentration peak but significantly broader onset for the 200 μM NaHS peak. Following incubation, the solution with a starting concentration of 100 μM had a final absorbance peak of 330 nm. At other time points during incubation, no other peaks between these two positions were noted, Figure 4. The solution with a starting concentration of 200 μM also has a main peak at 330 nm, but a smaller shoulder at 350 nm also appeared. Again, no other peaks were noticed between these two points. This is not the type of growth observed during our enzymatic synthesis, where the peak shifts continuously with time, even at the initially low concentrations of H_2S produced by CSE during the first 60 minutes, which are on the order of 50-100 μM. Therefore, we believe the continuous generation of H_2S by CSE must play a significant role in nanocrystal growth.

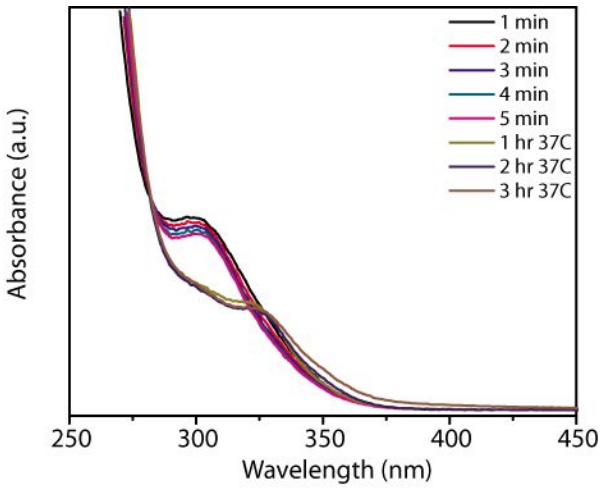

Figure 4. The absorbance spectra as a function of time for a solution of 1 mM Cd, 100 μM NaHS, and 8 mM L-cysteine in 0.1 M Tris buffer at pH 7.5 following rapid addition of NaHS and ripening at 37°C. The initial 5 minutes at room temperature are shown to demonstrate that the initial changes are very slow.

To more closely mimic the effect of constant generation of H_2S by CSE, we titrated NaHS in 2 μM aliquots over 2 hours to a final concentration of 500 μM. Figure 5 shows the absorbance spectra recorded at 20 μM NaHS increments, that is, every 10 aliquots. In contrast to Figures 3 and 4, the absorbance peak shifts continuously, even at low concentrations, indicative of growth by sequential addition of monomers to the growing particles. The absorbance intensity also increases over time, signifying an increase in overall particle concentration during growth. Both trends are generally reflected

in the optical properties during growth by biomineralization. Estimated particle sizes and HWHM values were calculated for corresponding absorbance spectra from Figure 5, shown in the inset of Figure 5 a) and Table S3. The size distributions were slightly larger at smaller particle size for the titrated addition as compared to direct addition case; however, they were similar at larger particle size. For example, the HWHM values for absorbance peaks at 330 and 350 nm were 31.2 $\pm$ 2.75 and 23 $\pm$ 2.0 for the titrated case and 24.2 $\pm$ 1.9 and 23.3 $\pm$ 2.0 for the biomineralization case, respectively. The small increase in size distribution may be due to a lower growth temperature, as the titrated samples are prepared at room temperature and the biomineralized samples are prepared at 37° C.

The total particle mass is quantifiable, by determining the concentration of nanocrystals from the peak absorbance intensity, and multiplying it by the average nanocrystal mass, which itself is calculated assuming spherical particles with density equal to the bulk density of CdS**.** The concentrations were calculated based on the size dependent relation reported by Yu *et al*.[30] The calculated mass values for instantaneous addition and titrated addition are presented in Figure 5 b). As expected, both the instantaneous addition and titrated addition samples show a linear increase in CdS mass with amount of NaHS added. However, the titrated addition sample has higher mass values for the same concentrations of NaHS. This is likely due to the availability of fresh precursor in solution, which not only allows growth of pre-existing particles by monomer addition, but causes the nucleation of new particles which will quickly grow to the average nanocrystal size. The accelerated growth of small nanocrystals compared to larger nanocrystals is expected for growth in the size focusing regime, where monomer species can diffuse quickly to the surface of the forming nanoparticles.[34]

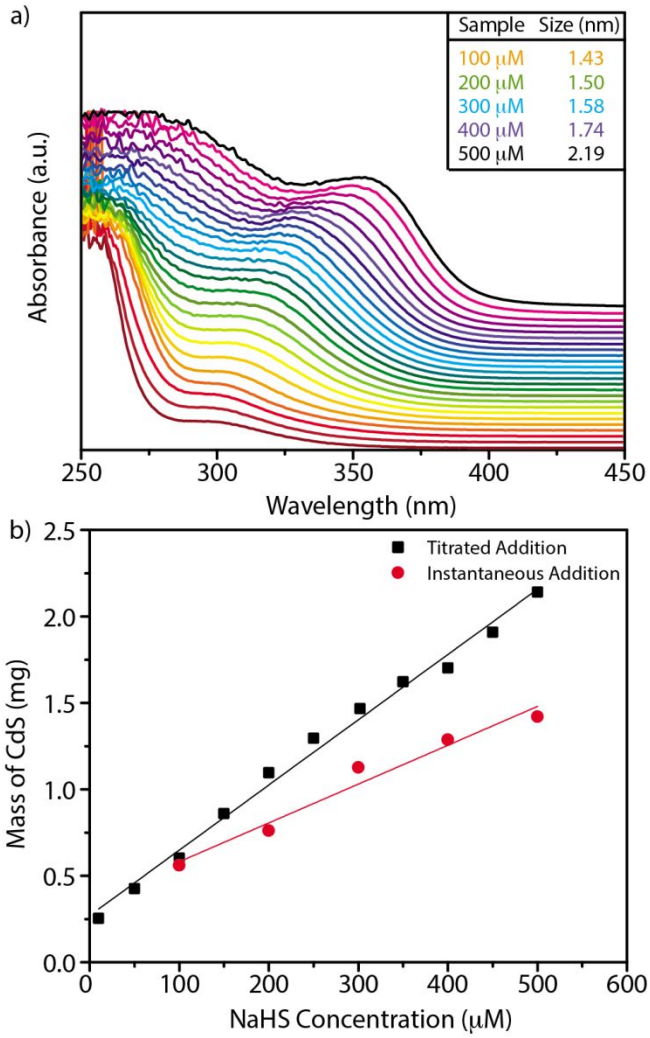

Figure 5. a) Absorbance spectra recorded after the stepwise addition of 20 μM NaHS for a solution of 1 mM cadmium and 8 mM L-cysteine in 0.1 Tris buffer, pH 7.5. b) Calculated total CdS mass for both titrated addition and instantaneous addition (values from Figure 2 a).

The TEM particle size distributions were measured for those populations with similar particle sizes, and thus similar absorbance peak wavelengths, corresponding to CdS QDs synthesized via biomineralization and are shown in Figure 6. The average particle sizes were 2.06 ± 0.45 nm and 2.44 ± 0.46 nm for sample populations with absorbance peak values of 330 nm and 350 nm, respectively. The nanocrystal diameters are identical to the average particle sizes calculated for the biomineralized sample with the same absorbance peaks. This result definitively validates our conclusion that CdS nanocrystal growth via biomineralization is best mimicked by chemical synthesis using a titrated

addition method, and that slow monomer additions yields size-controlled nanocrystal populations with narrow size distributions.

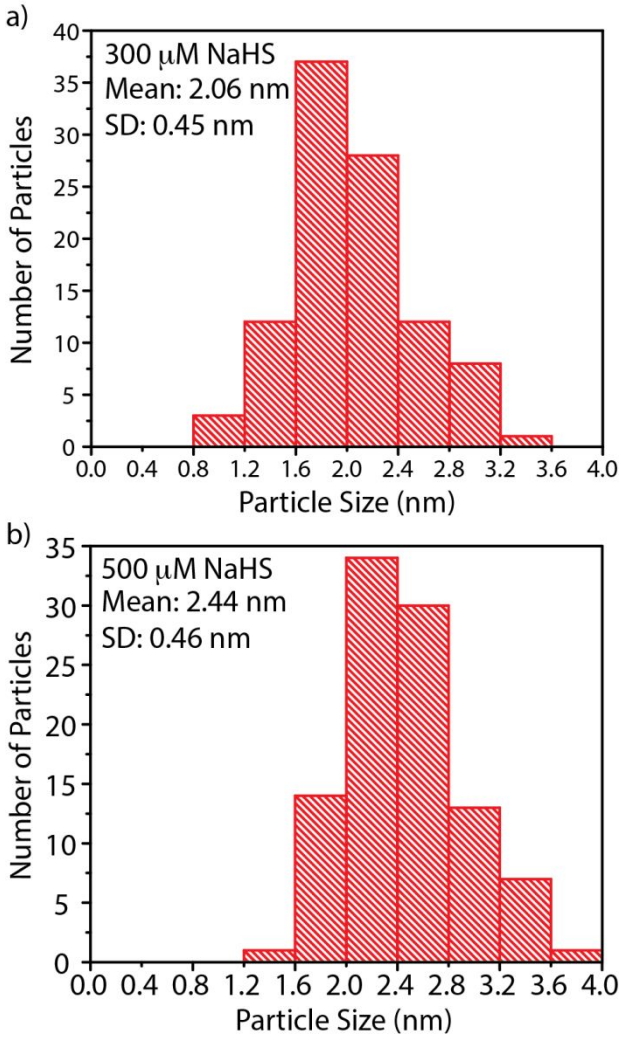

Figure 6. Particle size distributions for titrated addition chemical synthesis of CdS QDs corresponding to the populations from Figure 5 with UV-vis absorbance peaks at a) 330 nm and b) 350 nm.

To further demonstrate the influence of H_2S generation rate, and thus relative concentration of the limiting reactant, we increased the concentration of cadmium in solution during biomineralization. This approach to vary the Cd^{2+}: HS^- relative concentration was adopted because modifying the rate of enzymatically generated sulfur is not easily achieved. Figure 7 demonstrates the difference in absorbance spectra of CdS nanocrystals synthesized for 2 hours with varying cadmium acetate and L-cysteine concentrations using 0.05 mg/mL CSE. As demonstrated in both sets of data, an elevated cadmium concentration results in the formation of a higher concentration of smaller CdS nanocrystals,

indicated by a blue-shift in absorbance peak and increase in absorbance intensity relative to the typical growth conditions. A calculation of the estimated particle size based on absorbance peak confirms this result, showing a drop from 3.1 nm to 2.3 nm and 1.5 nm for nanocrystals synthesize using 1 mM Cd, 2 mM Cd, and 4 mM Cd respectively. A complete analysis of the estimated particle sizes and HWHM values are listed in Table S4. Increasing the amount of L-cysteine in solution has no effect on the change observed with increased cadmium concentration. This same phenomenon was also demonstrated by Priyam *et al.*, who saw the formation of smaller CdS nanocrystals with tighter size distributions at high cadmium concentrations independent of L-cysteine concentration under similar synthesis conditions.[35] Priyam attributed this effect to a high degree of cadmium supersaturation. Based on our results, cadmium concentration clearly plays a dominant role in determining the growth kinetics of the CdS nanocrystal populations.

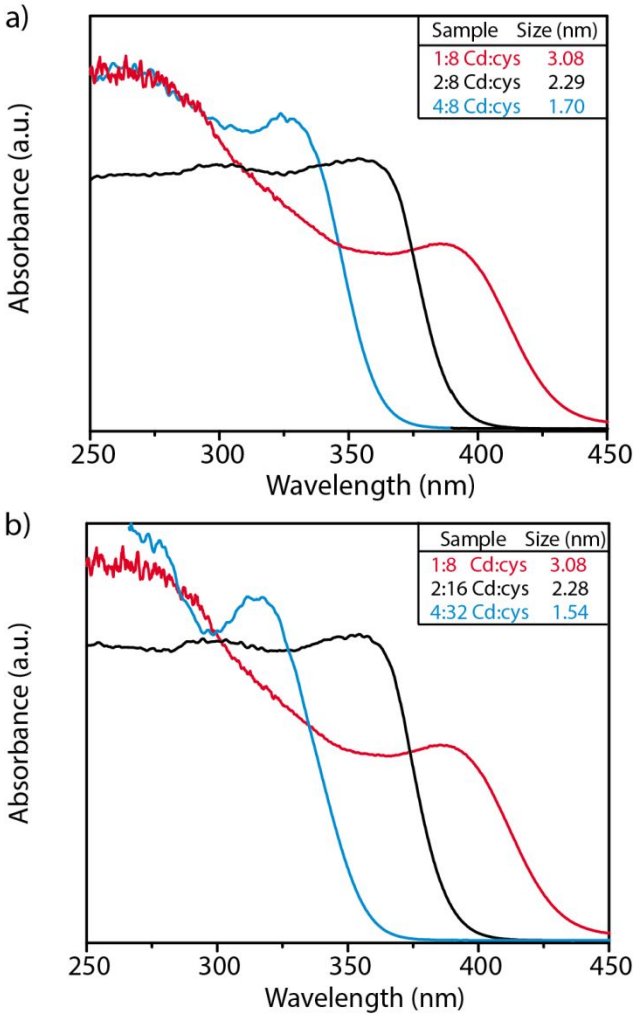

Figure 7. Absorbance spectra of CdS nanocrystal solutions synthesized at pH 7.5 with 0.05 mg/mL CSE for 2 hours for a) varied and b) the same cadmium:L-cysteine ratios.

Another important part of aqueous nanocrystal growth is the capping ligand, which plays a role in both growth and stabilization of the nanocrystals through the chelation of cadmium. We are not able to replace L-cysteine with another capping agent due to its additional role as a sulfur source. However, we were able to examine changes in the chelation strength of L-cysteine by varying the pH of enzymatic synthesis. L-cysteine is an amino acid with three side groups, each with its own pK_a value; amine, carboxylic acid, and thiol, with pK_a values of 8.7, 7.5, and 5.4 respectively. Previously in this work, CdS nanocrystals were synthesized at pH 7.5, meaning the carboxylic acid and thiol groups were deprotonated and available for binding. By raising the pH to 9, all the side groups will become deprotonated and bind more strongly to cadmium. Therefore, depending on the pH, L-cysteine will have a different chelating structure with cadmium, affecting both growth and particle stabilization.[36]

Figure 8 shows the absorbance and photoluminescence spectra as a function of time for CdS nanocrystals synthesized enzymatically in Tris buffer pH 9. A complete analysis of the estimated particle size, HWHM, and FWHM values are shown in Table S5. At pH 7.5, the CdS nanocrystals typically have an absorbance peak range of 330-390 nm, Figure 1. At pH 9, the peak range is reduced to between 370-390 nm, correlating to an average particle size of 2.45 – 2.71 nm. However, the CdS nanocrystals formed at pH 9 are stable for at least 2 weeks at 4 °C, whereas those produced at pH 7.5 are only stable for 1-3 days. The stronger binding of L-cysteine to cadmium at higher pH restricts the accessible size window of CdS nanocrystals, but improves capping of the particles and thus stability following growth. This change demonstrates that L-cysteine plays a major role in nanocrystal synthesis by binding strongly enough to prevent aggregation, but weakly enough to allow size-controlled growth of the nanoparticles. This moderate binding strength is advantageous for our synthesis because it allows us to tune nanocrystal size; however, this is unfavorable over long times due to L-cysteine's lack of stability in solution.

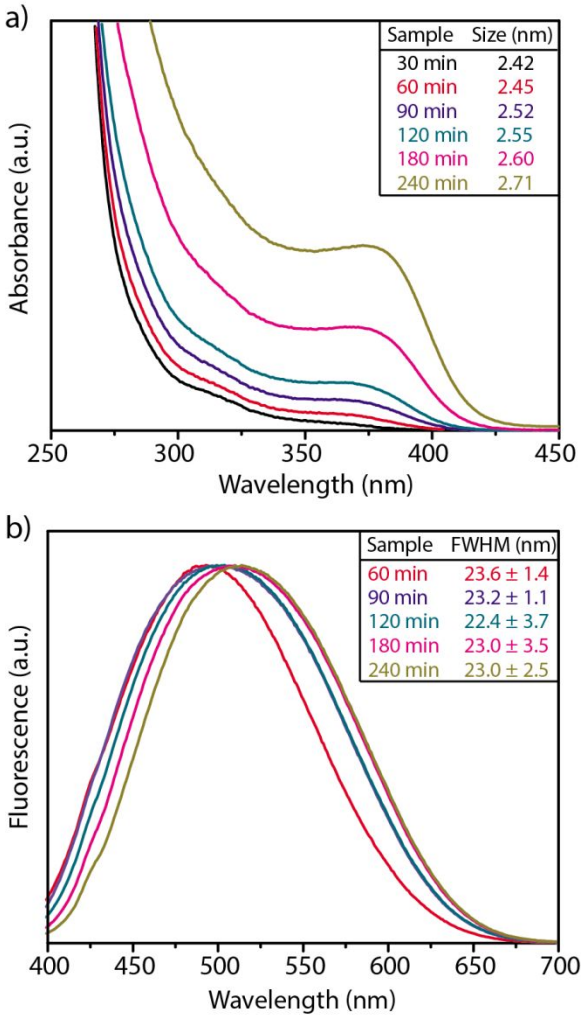

Figure 8. a) Absorbance and b) photoluminescence spectra of a solution of CdS quantum dots synthesized from 1 mM cadmium, 8 mM L-cysteine, 0.04 mg/mL CSE in pH 9 Tris buffer.

Discussion

The absorbance spectra corresponding to CdS nanocrystals grown by CSE, Figure 1, are best approximated by the results of the titrated chemical synthesis approach, Figure 5. Both the biomineralization approach and the titrated addition of NaHS to solution yields the formation of CdS nanocrystals with an average size that grows continuously over the synthesis period. In both cases, this is due to the sustained concentration of monomers, provided either by titrated NaHS addition or by the enzymatic turnover of L-cysteine to H_2S, allowing growth to proceed by continuous monomer addition during synthesis. Additionally, the results presented in both Figure 3 and 5 demonstrate the influence of total CdS concentration on the equilibrium nanocrystal size in solution. Increasing the relative amount of

NaHS in solution provides a more reactive precursor, allowing an increased production of CdS. This increased amount of CdS also causes an increase in the average nanocrystal size, as evidenced by a red-shift of the absorbance peak in solution.

Understanding these results requires a more detailed discussion of the theory of nanocrystal formation and growth. The most widely followed model for nanocrystal synthesis, proposed by LaMer *et al*., theorizes that colloidal particle formation occurs in three stages; namely, monomer accumulation, nucleation, and growth.[37] In most traditional nanocrystal syntheses, for example hot-injection, a burst of monomers are rapidly generated to produce an instantaneous oversaturation in solution, causing a fast nucleation event followed by slower growth. The kinetics of nucleation are complex, but have been modeled by applying the Gibbs-Thompson equation, which describes how a particle's solubility increases as its size decreases.[38]

$$S_d = S_\infty e^{\frac{4\sigma V_M}{dRT}} \quad (1)$$

Particle solubility S_d is a function of: S_∞, bulk solubility of the crystal; σ, the surface energy; V_M, the molar volume of the crystal; R, the gas constant; and T, absolute temperature. Nucleation will occur at the point where the chemical potential of a crystal with a certain diameter is equal to the chemical potential of a concentration of monomers at the solubility of the crystal. When nucleation occurs, this corresponds to a change in the free energy of the system, which can then be used to calculate a critical particle size, above which it is thermodynamically favorable for crystal formation and below which it is unfavorable, *i.e.* the crystal will dissolve. The full derivation has been reported elsewhere,[7, 38] and results in a critical radius (r_{crit}) as described below.

$$r_{crit} = \frac{8\sigma V_M}{3RTln(\omega)} \quad (2)$$

In the above equation, ω is the supersaturation, defined as the concentration of monomers over the solubility of a bulk crystal, [M]/ S_∞. The size of r_{crit} has a direct effect on the growth rate of nanocrystals in solution. For diffusion controlled growth, the growth rate for a population of nanocrystals in solution is given by

$$\frac{d(\Delta\bar{r})}{dt} = \frac{2\sigma V_m D S_\infty}{\bar{r}^2 RT}\left(\frac{1}{\bar{r}} - \frac{1}{r_{crit}}\right) \quad (3)$$

In the above equation, $\bar{r}$ is the average crystal size, and D is the diffusion constant. There is also a growth equation for reaction limited growth, however, the monomers in our solutions are relatively dilute overall and therefore the diffusion limited case is more appropriate. Based on this equation, when

the average particle size is larger than the critical radius, i.e. $\frac{\bar{r}}{r_{crit}} \geq 1$, the size distribution will narrow, or focus. Once the critical size is larger, $\frac{\bar{r}}{r_{crit}} < 1$, the size distribution will broaden. Physically, these two cases correspond to two different conditions in solution that we have qualitatively discussed in the previous section. In the focusing regime, the monomer concentration is still high enough to diffuse towards the already formed nanocrystals, resulting in overall growth. In this case, the small particles will grow quickly and the larger particles will grow slowly, leading to a narrowing of the size distribution. Once the concentration of monomers in solution drops, the critical radius increases and particles smaller than this critical radius will dissolve, supplying monomers to the larger particles to continue growth. This effect, known as Ostwald ripening, leads to a broadening of the size distribution as the smaller particles begin to dissolve and only the larger particles continue to grow.

Putting our results into this framework, the slow enzymatic production of H_2S by CSE results in a consistent supply of monomers, and thus a high supersaturation term that is sustained throughout growth. This yields a small critical radius for nanocrystals in solution, driving the growth behavior to be size focusing throughout the growth time. Quantifying the degree of supersaturation, ω, allows for a better understanding of the effect of monomer concentration on the critical radius. ω can be calculated by dividing the monomer concentration by S_∞, or bulk crystal solubility. S_∞ can be calculated in terms of the anion species HS^- to allow a simple calculation of supersaturation given the generation of HS^- in solution. S_∞ for the bulk crystal would traditionally be calculated using the solubility constant for CdS (K_{sp}), however, the presence of ligands in solution will affect the solubility and must also be considered, yielding a new solubility constant, K_{obs}. This was calculated for our system following the procedure of Xie *et al*, and is shown in detail in the supporting information.[38] Based on the calculation for our system, S_∞ = 0.047 μM in terms of HS^- for a cadmium concentration of 1 mM. In water, H_2S will dissociate into HS^- and H^+. This dissociation is favorable at pH > 7, and any H_2S in solution will completely dissociate; thus $[H_2S] = [HS^-]$.[39] Based on this result, any concentration of H_2S in solution which is greater than 0.047 μM will result in nucleation. This is well below our estimated concentration of H_2S generated by CSE, ~4 μM/min.

Another key value of interest is the critical radius corresponding to a specific degree of supersaturation. Several groups have demonstrated that the term $\frac{2\sigma V_M}{RT}$ is typically ≤1 for diffusion controlled conditions.[9, 38] The low bulk solubility, S_∞= 0.047 μM in terms of HS^-, will result in a high supersaturation term (ω), which tends to dominate the r_{crit} calculation.[34, 35] Using the S_∞ value calculated previously, we can estimate that for our system in the presence of 1 mM cadmium acetate at

pH 7.5, r_{crit} will range from 0.58 nm for the case of 100 μM NaHS to 0.30 nm for 500 μM NaHS. These results indicate that the reintroduction of monomers, even at low levels such as 100 μM NaHS, result in a critical radius much smaller than the average particle size, allowing growth to occur in the size focusing regime. Using the estimated r_{crit} values, $\frac{d(\Delta\bar{r})}{dt}$, or the rate of change to the size distribution over time, can be estimated given an average nanocrystal size. For the base case of 1 mM Cd acetate at pH 7.5, $\frac{d(\Delta\bar{r})}{dt}$ ranges from -0.13 to -0.017 for $\bar{r}$ equal to 1 nm and 4 nm, respectively. This result verifies the size focusing behavior observed throughout our growth process. Additionally, the more negative $\frac{d(\Delta\bar{r})}{dt}$ value observed for a smaller average particle size demonstrates that smaller particles will have a stronger rate of size focusing than populations with larger diameters, which change more slowly.

Given the theory discussed, we are now able to describe a hypothetical mechanism of nanocrystal growth for our biomineralization process. When CSE is added to solution, it begins to turn over L-cysteine to H_2S at an approximate rate of 4 μM/min. At pH 7.5, H_2S will immediately dissociate into HS^-, and any concentration of HS^- > 0.047 μM will result in the formation of CdS nanocrystals. This means CdS nanocrystals will be nucleated almost instantaneously and enter the growth phase. While the reaction of HS^- and Cd occurs quickly and would ordinarily lead to rapid consumption of HS^-, the continuous generation of HS^- in solution sustains the monomer concentration, allowing growth to proceed in the size focusing regime. This is represented mathematically by a sustained supersaturation of monomers (ω), which drives the critical radius (r_{crit}) to be smaller than the average nanocrystal size, meaning $\frac{\bar{r}}{r_{crit}} \geq 1$ which causes $\frac{d(\Delta\bar{r})}{dt}$ to be negative. In this regime, even if new nanocrystals are nucleated, they will have an accelerated growth rate compared to pre-existing particles due to their much smaller size.

While our biomineralization growth mechanism was developed and tested using a chemical synthesis method, we were able to confirm the growth dependence on supersaturation by altering the concentration of cadmium during enzymatic growth. Figure 7 demonstrates that increasing the cadmium concentration by either a factor of two or four results in the growth of a large number of particles with a much smaller size over the same amount of time. In the context of equations 2 and 3, the supersaturation of monomers would also be two or four times as large for the same HS^- concentration. Given an NaHS concentration of 100 μM, this corresponds to a critical radius of 0.41 and 0.32 nm for 2 mM Cd and 4 mM Cd, respectively. These smaller critical radius values will drive the average radius to tend towards smaller values over time, resulting in a population of smaller particles.

In the absence of a continuous supply of HS^-, growth will occur differently following the introduction of precursors, as observed in Figure 3. At a HS^- concentration $\geq$ 300 μM, continuous growth by monomer addition in the size focusing regime is still observed. However, at HS^- concentrations $\leq$ 200 μM, discrete absorbance peaks indicating specific nanocrystal sizes are observed. Vossmeyer *et al.* observed the same growth behavior under similar conditions and attributed this to two possibilities. The first is growth by coalescence, which occurs when pre-existing nucleated particles attach to neighboring particles. The second possibility is that certain particle sizes are more thermodynamically favorable; for example, the peaks at ~300 nm and ~330 nm correspond to particle sizes which are the most thermodynamically stable in solution.[33] In either case, the observation of discrete peaks is only possible in the absence of fresh monomers in solution. As our enzymatic synthesis has constant introduction of precursors, this type of growth is not applicable to our system.

The capping agent L-cysteine also plays an important role in determining the size and stability of CdS particles. Figure 8 demonstrates that CdS nanocrystals synthesized at pH 9 grow to a much larger initial size and also have a more restricted size window of growth. This change most likely has to do with the interaction between cadmium and L-cysteine. An increase in chelating strength as a function of pH affects the final size of the CdS nanocrystals by changing the surface energy term in equations 2 and 3. Given the complexity of calculating surface energy, we are not able to quantify this change. However, the effect is clearly seen in the absorbance spectra for the CdS quantum dots formed in Figure 8. An additional term that may be affected in equation 2 is the bulk solubility, which is dependent on the K_a of all possible Cd-cysteine complexes in solution. However, this change would not be as significant as the change in surface energy of the crystals.

Over time, L-cysteine will form the dimer L-cystine, which is insoluble in solution. As the overall L-cysteine concentration drops, the CdS nanocrystals will begin to precipitate out of solution. The effect is noticed more rapidly at pH 7.5 than at pH 9 as cadmium binding is not as strong at a lower pH. Therefore, L-cysteine is a good choice for nanocrystal growth, but does not allow long term particle stability. Alternative thiol capping agents, such as mercaptopropionic acid (MPA), have been shown to have better long-term stability for aqueous cadmium chalcogenide quantum dots. However, the use of supplementary thiols in our aqueous synthesis has been shown to slow down growth dramatically, and more than 24 hours are required to form any nanocrystals in solution at 37 °C. Additionally, it is difficult to achieve larger sized particles due to the strength of capping.

Conclusions

This work explains the mechanism by which biomineralization can yield size-controlled nanomaterials, with the case study of aqueous phase CdS nanocrystal nucleation and growth at room temperature via a single enzyme approach. The aqueous phase enzymatic turnover of L-cysteine to form H_2S initiates nucleation by reaction of the formed HS^- ions with Cd^{2+} ions in solution. This relatively slow, but steady, generation of the active precursor results in a high, sustained supersaturation of monomer during growth, resulting in a critical radius on the order of 0.3-0.6 nm. This places the growth mechanism firmly within the size focusing regime of crystal growth, where the critical radius is smaller than the average nanocrystal size. This route to controlled nanocrystal populations can be replicated through slow, titrated addition of reactive NaHS in a purely chemical, aqueous-phase, synthesis approach. The particle size distribution can be controlled by manipulating the degree of supersaturation during enzymatic synthesis through the cadmium concentration. Additional control can be achieved through tuning the L-cysteine capping agent binding strength via the synthesis solution pH, with higher pH, and thus higher binding strength leading to larger, more stable particles at the expense of growth rate.

Acknowledgements

This material is based upon work supported by the National Science Foundation under the programs EFRI-PSBR, Grant No. 1332349, and SNM-IS, grant number 1727166. We thank Dr. Angela Brown of the Department of Chemical Engineering for use of the fluorometer. We also thank Li Lu of the Material Science Department for acquiring TEM images of the CdS nanocrystals.

References

1 C. B. Murray, D. J. Norris and M. G. Bawendi, *J. Am. Chem. Soc.,* 1993, **115**, 8706-8715.

2 C. B. Murray, C. R. Kagan and M. G. Bawendi, *Annu. Rev. Mater. Sci.,* 2000, **30**, 545-610.

3 P. Reiss, *Semiconductor Nanocrystal Quantum Dots*, ed. A. Rogach, Springer, 2008, p. 35-72.

4 R. Dunleavy, L. Lu, C. J. Kiely, S. McIntosh and B. W. Berger, *Proc. Natl. Acad. Sci.,* 2016, **113**, 5275-5280.

5 X. Peng, J. Wickham and A. Alivisatos, *J. Am. Chem. Soc.,* 1998, **120**, 5343-5344.

6 H. Reiss, *J. Chem. Phys.,* 1951, **19**, 482-487.

7 D. V. Talapin, A. L. Rogach, M. Haase and H. Weller, *J. Phys. Chem. B,* 2001, **105**, 12278-12285.

8 A. Priyam, A. Chatterjee, S. C. Bhattacharya and A. Saha, *J. Cryst. Growth,* 2007, **304**, 416-424.

9 L. Jing, S. V. Kershaw, Y. Li, X. Huang, Y. Li, A. L. Rogach and M. Gao, *Chem. Rev.,* 2016, **116**, 10623-10730.

10 X. Huang, L. Jing, S. V. Kershaw, X. Wei, H. Ning, X. Sun, A. L. Rogach and M. Gao *J. Phys. Chem. C,* 2018, **122**, 11109-11118.

11 W. J. Parak, D. Gerion, T. Pellegrino, D. Zanchet, C. Micheel, S. C. Williams, R. Boudreau, M. A. Le Gros, C. A. Larabell and A. P. Alivisatos, *Nanotechnology,* 2003, **14**, R15.

12 F. Nudelman and N. A. Sommerdijk, *Angew. Chem., Int. Ed.,* 2012, **51**, 6582-6596.

13 C. Dameron, R. Reese, R. Mehra, A. Kortan, P. Carroll, M. Steigerwald, L. Brus and D. Winge, *Nature*, 1989, **338,** 596-597.

14 M. Fauchon, G. Lagniel, J. Aude, L. Lombardia, P. Soularue, C. Petat, G. Marguerie, A. Sentenac, M. Werner and J. Labarre, *Mol. Cell,* 2002, **9**, 713-723.

15 D. Pages, J. Rose, S. Conrod, S. Cuine, P. Carrier, T. Heulin and W. Achouak, *PLoS One,* 2008, **3**, e1539.

16 H. Bai, Z. Zhang, Y. Guo and G. Yang, *Colloids Surf., B,* 2009, **70**, 142-146.

17 F. Liu, S. H. Kang, Y. Lee, Y. Choa, A. Mulchandani, N. V. Myung and W. Chen, *Appl. Phys. Lett.,* 2010, **97**, 123703.

18 W. Zhou, D. T. Schwartz and F. Baneyx, *J. Am. Chem. Soc.,* 2010, **132**, 4731-4738.

19 Z. Yang, L. Lu, C. J. Kiely, B. W. Berger and S. McIntosh, *ACS Appl. Mater. Interfaces,* 2017, **9,** 13430–13439.

20 L. C. Spangler, L. Lu, C. J. Kiely, B. W. Berger and S. McIntosh, *J. Mater. Chem. A,* 2016, **4**, 6107-6115.

21 A. Sadeghnejad, L. Lu, C. J. Kiely, B. W. Berger and S. McIntosh, *RSC Adv.,* 2017, **7**, 38490-38497.

22 L. C. Spangler, R. Chu, L. Lu, C. J. Kiely, B. W. Berger and S. McIntosh, *Nanoscale,* 2017, **9**, 9340-9351.

23 V. Lesnyak, N. Gaponik and A. Eychmüller, *Chem. Soc. Rev.,* 2013, **42**, 2905-2929.

24 Z. Yang, L. Lu, C. J. Kiely, B. W. Berger and S. McIntosh, *Ind. Eng. Chem. Res.* 2016, **55**, 11235-11244.

25 M. K. Thorson, T. Majtan, J. P. Kraus and A. M. Barrios, *Angew. Chem., Int. Ed.,* 2013, **52**, 4641-4644.

26 T. Chiku, D. Padovani, W. Zhu, S. Singh, V. Vitvitsky and R. Banerjee, *J. Biol. Chem.,* 2009, **284**, 11601-11612.

27 A. E. Martell and R. M. Smith, *Critical Stability Constants*, Springer, 1974.

28 W. Liu, H. S. Choi, J. P. Zimmer, E. Tanaka, J. V. Frangioni and M. Bawendi, *J. Am. Chem. Soc.,* 2007, **129**, 14530-14531.

29 Z. Yang, L. Lu, V. F. Berard, Q. He, C. J. Kiely, B. W. Berger and S. McIntosh, *Green Chem.,* 2015, **17**, 3775 -3782.

30 W. W. Yu, L. Qu, W. Guo and X. Peng, *Chem. Mater.,* 2003, **15**, 2854-2860.

31 M. Wang, W. Cai, N. Li, Y. Ding, Y. Chen and Y. Zhu, *Antioxid. Redox Signaling,* 2010, **12**, 1065-1077.

32 L. Li, M. Bhatia, Y. Z. Zhu, Y. C. Zhu, R. D. Ramnath, Z. J. Wang, F. B. M. Anuar, M. Whiteman, M. Salto-Tellez and P. K. Moore, *FASEB J.,* 2005, **19**, 1196-1198.

33 T. Vossmeyer, L. Katsikas, M. Giersig, I. G. Popovic, K. Diesner, A. Chemseddine, A. Eychmueller and H. Weller, *J. Phys. Chem.,* 1994, **98**, 7665-7673.

34 N. T. K. Thanh, N. Maclean and S. Mahiddine, *Chem. Rev.,* 2014, **114**, 7610-7630.

35 A. Priyam, S. Ghosh, A. Datta, A. Chatterjee and A. Saha, *Recent Trends in Surface and Colloid Science*, ed. Satya Moulik, World Scientific Publishing Company, 2014, 271-296.

36 F. Jalilehvand, B. O. Leung and V. Mah, *Inorg. Chem.,* 2009, **48**, 5758-5771.

37 V. K. LaMer and R. H. Dinegar, *J. Am. Chem. Soc.,* 1950, **72**, 4847-4854.

38 R. Xie, Z. Li and X. Peng, *J. Am. Chem. Soc.,* 2009, **131**, 15457-15466.

39 H. Weller, *Angew. Chem., Int. Ed.,* 1993, **32**, 41-53.

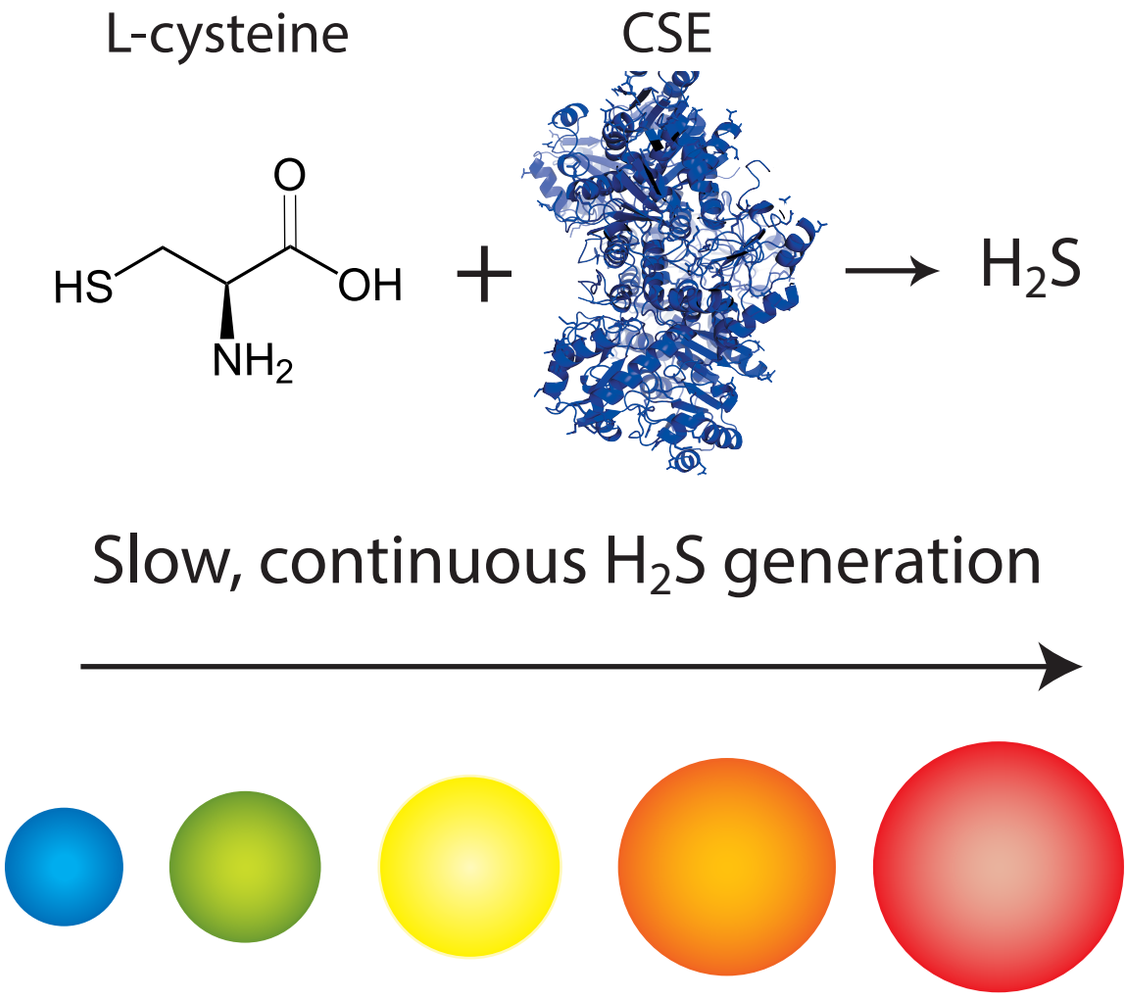
L-cysteine
CSE
HS
O
OH
NH2
H2S
Slow, continuous H2S generation

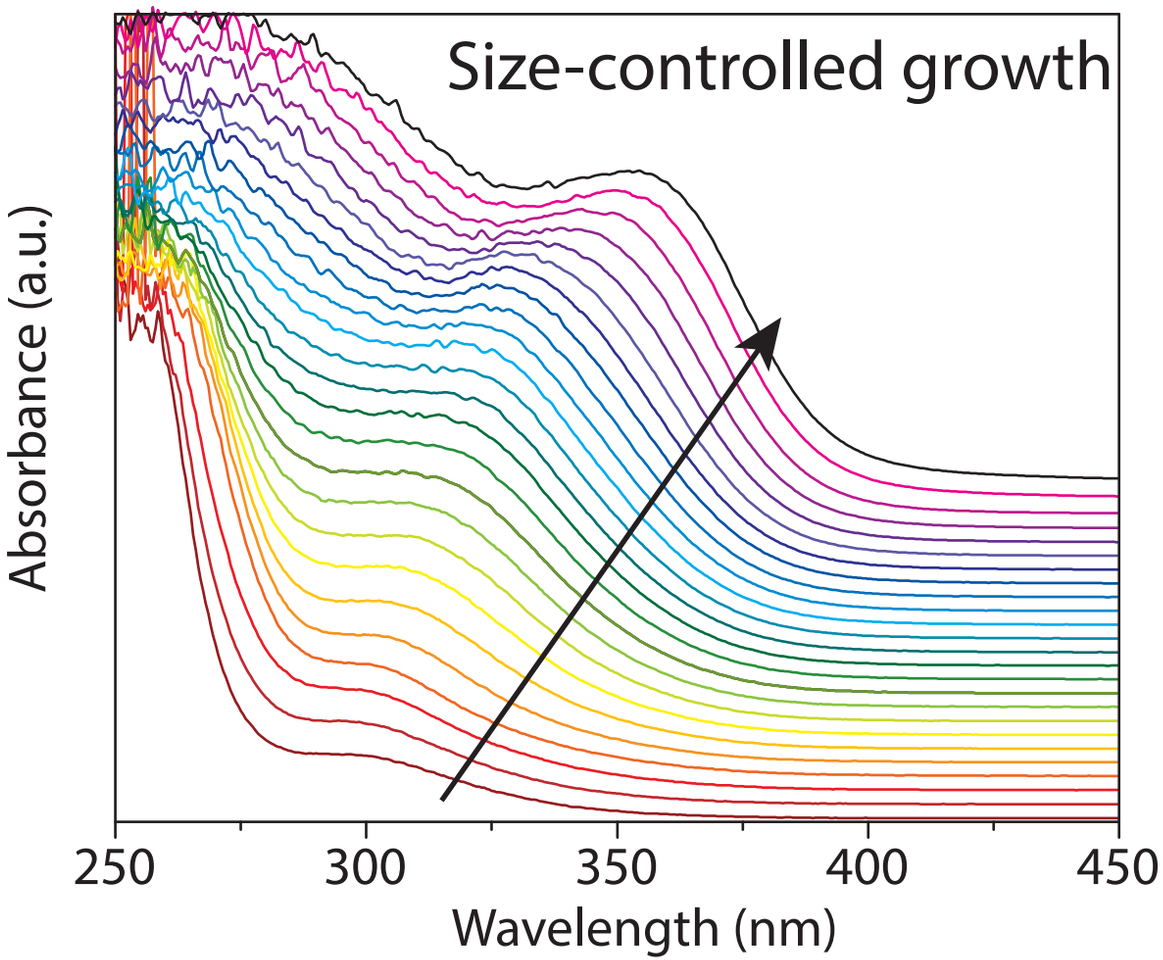
Size-controlled growth
Absorbance (a.u.)
250
300
350
400
450
Wavelength (nm)